

# Self-Suspended Nanoparticles for N-Alkylation Reactions: A New Concept for Catalysis

Maria Sarno,\* Claudia Cirillo, and Mariagrazia Iuliano<sup>[a]</sup>

The catalytic activity of snowman-like and core-shell Fe<sub>3</sub>O<sub>4</sub>/Au nanoparticles (NPs), obtained through a “wet chemistry” approach which directly restitutes nanocatalysts stable and highly active in the reaction medium, was tested towards N-alkylation reactions. The nanocatalysts were tested for the synthesis of secondary amines. The core-shell NPs, thanks to the

surface properties, homogeneous dispersion and intimate connection with reagents in the catalyst medium, exhibited an excellent catalytic activity (e.g. >99% yield and conversion of aniline in very short time and mild conditions). Owing to the magnetic part, the nanoparticles can be easily separated and reused, showing an almost stable activity after 10 cycles.

## 1. Introduction

Different agrochemicals, pharmaceuticals, bioactive and natural identical molecules are produced from intermediates such as N containing molecules, e.g. amines.<sup>[1]</sup> For the syntheses various approaches have been proposed and developed.<sup>[2–7]</sup> The so called borrowing hydrogen method, consisting in an alcohol based alkylation, is a very promising approach for the synthesis of secondary amines<sup>[8–17]</sup> attracting recently great attention.<sup>[11,12,18–25]</sup> Indeed, it is an atom-economic and environmental friendly approach, as alcohols are abundant and water is the only by-product. Homogeneous catalysts have been extensively studied<sup>[26–40]</sup> and catalysts based on Ru,<sup>[21]</sup> Ir,<sup>[41]</sup> Pd,<sup>[42]</sup> Au,<sup>[43]</sup> Pt<sup>[44]</sup> have been successfully used. On the other hand, homogeneous catalysts suffer from some typical drawbacks such as recovery, handling of metal complexes, etc. Homogeneous catalysts recovery is a key topic in industrial chemistry. Also, heterogeneous catalysis has been explored.<sup>[21–25,45–59]</sup> Heterogeneous catalysts containing metals such as Pd,<sup>[21–25]</sup> Ru,<sup>[45]</sup> Au,<sup>[46]</sup> Ag<sup>[47–48]</sup> and Fe<sup>[58,59]</sup> have been used for N-alkylation of amines with alcohols. However, they require multistep and complex procedures and often result in reduced activity and selectivity. Indeed, good activity can be achieved at temperatures higher than 140 °C.<sup>[26,32–39,43,46,50–59]</sup> This is mainly due to diffusion limitations and heterogeneity of the active sites. Nanoparticles (NPs) because of size and surface area are ideal candidates to support catalysts, suppling large load and improved activities. On the other hand, the design and develop-

ment of an easy recoverable and/or recyclable nanocatalysts can reduce environmental impact and costs.

Surface modifications<sup>[60–62]</sup> can provide an hydrophobic nature to stable nanoparticles in reaction media, avoiding agglomeration and aggregation. Although, it is so promising, there are few examples of catalysis promoted by self-suspended nanoparticles and none, at the best of our knowledge, to promote N-alkylation reactions. In recent years, magnetically recyclable nano-catalysts have attracted much attention in organic synthesis. Apart from an ease of separability, they also have other advantages such as low toxicity simple preparation technique and are low-cost. [1] The magnetic nano-catalyst can broadly be divided into two types: (i) supported magnetic nano-catalyst, the active metal is deposited on freshly prepared Fe<sub>3</sub>O<sub>4</sub> nano-material, and (ii) a mixed ferrite nano-catalyst with general formula MFe<sub>2</sub>O<sub>4</sub> (where M is a divalent cation other than iron), all starting materials are incorporated into one pot. [2] Gold catalysts, that had been for long time considered inert, have obtained considerable attention because of the catalytic activity and selectivity showed at the small sizes.<sup>[43]</sup> This activity strongly depends on: the particles size; crystallographic nature,<sup>[63]</sup> etc... In particular, gold has been found to exhibit unique catalytic properties for a number of liquid and vapor phase reaction.<sup>[64]</sup> Moreover, magnetite is a soft Lewis acid in organic synthesis<sup>[58,64,65]</sup> and can catalyze N-alkylation reaction, e.g. through hydrogen autotransfer.<sup>[58,59]</sup>

Here we report, for the first time, the catalytic activity towards N-alkylation reactions of Fe<sub>3</sub>O<sub>4</sub>/Au snowman-like (Fe<sub>3</sub>O<sub>4</sub>/AuSM) and Fe<sub>3</sub>O<sub>4</sub>/Au core-shell (Fe<sub>3</sub>O<sub>4</sub>/AuCS) NPs. They were obtained through a “wet chemistry” approach, which is a scalable and reliable synthesis method. It directly restitutes nanoparticles stable in solution, without requiring further modification,<sup>[62,66–68]</sup> thanks to the surfactant molecules covering the NPs during synthesis and allowing a behaviour between homogeneous and heterogeneous catalysis. In particular, the NPs can be dispersed and stabilized in solution because of the small size and the ligand coating, whereas magnetic part allows easily separation.

The two different nanocatalysts were prepared to explore: ligand covered nanometric size gold surfaces; and heterojunc-

[a] Prof. M. Sarno, Dr. C. Cirillo, Dr. M. Iuliano  
Department of Industrial Engineering and Centre NANO\_MATES  
University of Salerno  
Via Giovanni Paolo II, 132-84084 Fisciano (SA), Italy  
E-mail: msarno@unisa.it

Supporting information for this article is available on the WWW under <https://doi.org/10.1002/open.201900104>

©2019 The Authors. Published by Wiley-VCH Verlag GmbH & Co. KGaA.  
This is an open access article under the terms of the Creative Commons Attribution Non-Commercial NoDerivs License, which permits use and distribution in any medium, provided the original work is properly cited, the use is non-commercial and no modifications or adaptations are made.

tion between small gold NPs on magnetite, reducing the amount of noble metals too.

In particular, N-alkylation of aniline and other substrates as alkylating agent, were investigated, showing in the case of core-shell NPs very high conversion and selectivity in short times and mild conditions.

## Experimental Section

### Materials

The synthesis process for magnetic snowman-like  $\text{Fe}_3\text{O}_4/\text{AuSM}$  NPs was modified based on the Hao et al. method<sup>[66,69,70]</sup> and performed in the experimental apparatus shown in Figure 1a. 2-propanol and hexane were used as received. 1-octadecene (90%), oleic acid (OA), 1,2-hexadecanediol (90%), iron(III) acetylacetonate ( $\text{Fe}(\text{acac})_3$ ) (97%) and gold(III) chloride trihydrate ( $\text{HAuCl}_4$ ) were acquired from Aldrich Chemical Co. For the preparation of  $\text{Fe}_3\text{O}_4/\text{AuSM}$ : 20 mL of 1-octadecene, 2 mmol of  $\text{Fe}(\text{acac})_3$ , 0.1 mmol of  $\text{HAuCl}_4$ , 10 mmol of 1,2-hexadecanediol, 12 mmol of oleic acid were mixed and heated from 25 °C to 190 °C for 2 h and then to 275 °C for 1 h. For washing,

centrifugations (7500 rpm; 0.5 h) in ethanol and then in a mixture of 2-propanol and hexane (2:1 v/v) were performed.

The synthesis process for magnetic core-shell  $\text{Fe}_3\text{O}_4/\text{Au}$  NPs, named in the following  $\text{Fe}_3\text{O}_4/\text{AuCS}$ , or  $\text{Fe}_3\text{O}_4/\text{AuCS@OA}$  to highlight the complexation with the organic coating, was performed in the same experimental apparatus as previously described.<sup>[71]</sup> In particular, the magnetic  $\text{Fe}_3\text{O}_4$  NPs were synthesized as previously reported elsewhere.<sup>[70]</sup>

The as-prepared  $\text{Fe}_3\text{O}_4$  NPs were dispersed in hexane. For Au coating, in a typical experiment, 2.5 mmol of  $\text{HAuCl}_4 \cdot 3\text{H}_2\text{O}$  were dissolved in 10 mL chloroform, 9 mL of  $\text{NaBH}_4$  and 1 mmol OA. Another 10 mL chloroform solution, containing 40 mg of 10 nm  $\text{Fe}_3\text{O}_4$  NPs and 2 mmol of OA, was prepared. Under stirring, the  $\text{HAuCl}_4$  solution was added dropwise into the  $\text{Fe}_3\text{O}_4$  NPs solution. After 20 h, the Au coated  $\text{Fe}_3\text{O}_4$  NPs were precipitated by adding ethanol and washed by hexane and ethanol for several times.

### Procedure for N-Alkylation

In a typical experiment, a mixture of 1.0 mmol of substrate (aniline, 2-aminobenzothiazole, 2-aminopyridine, 4-methoxyaniline, 2-methylaniline and 3-chloroaniline), 1 mmol of alcohol (benzyl alcohol, 4-methylbenzyl alcohol,  $\alpha$ -methylbenzyl alcohol, 2-methyl-2-propanol and 1-octanol),  $\text{Cs}_2\text{CO}_3$  (2.0 mmol), toluene (5 mL) and 1 mg of nanocatalyst was taken in a 50 mL round bottomed flask and stirred at 100 °C for 4 h. The reaction was carried out under  $\text{N}_2$  atmosphere. The progress of the catalytic reactions was monitored through GC analysis, which was performed on the reaction mixtures at different time intervals. Before measurements, the catalyst was separated under a magnetic field and the reaction mixture cooled. Then the mixture was passed through anhydrous  $\text{Na}_2\text{SO}_4$  and dried under vacuum, or only dried. The products were identified by GC analysis.<sup>[32,72-74]</sup>

Qualitative analysis was compared with chromatographic standard and mass spectrometry of the product. The obtained results were in good agreement with parallel evaluation performed by using dodecane as internal standard.<sup>[51,52]</sup> No substantial differences were observed for the samples differently pretreated. The experiments were performed in triplicate. Along the results the text are expressed with a standard deviation, which takes into account the different tests.

The conversion of amine was calculated as follows:

$$\text{Conversion (\%)} \text{ of amine} = \frac{\text{Initial wt.\% of amine} - \text{final wt.\% of amine}}{\text{Initial wt.\% of amine}} * 100$$

### Characterization Techniques

XRD measurements were performed with a Bruker D8 X-ray diffractometer using  $\text{CuK}\alpha$  radiation. Thermogravimetric analysis (TG-DTG) at 10 K/min heating rate in air flow was performed with a SDTQ 600 Analyzer (TA Instruments). Transmission electron microscopy (TEM) images were acquired using a FEI Tecnai electron microscope operated at 200 KV with a  $\text{LaB}_6$  filament as the source of electrons, equipped with an energy dispersive X-ray (EDX) probe. The N-alkylation of amines using alcohols, after a purification by a chromatographic column, were analyzed through a GC-MS (Thermo Fischer Scientific) equipped with HP-5 capillary column ( $0.25 \mu\text{m} \times 0.25 \text{mm} \times 30 \text{m}$ ). All reaction products were identified by matching the GC retention time with authentic samples. The column temper-

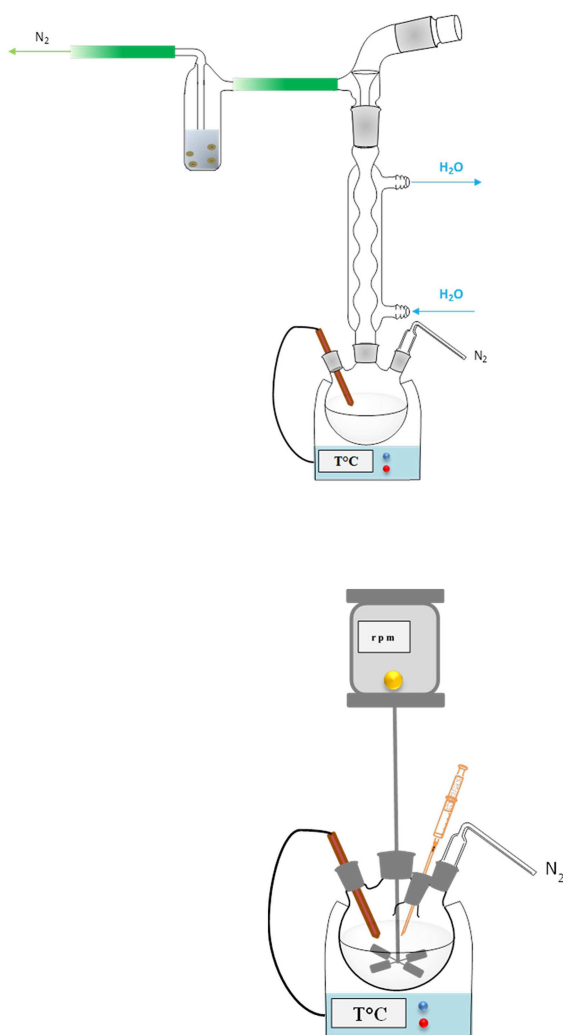


**Figure 1.** Schemes of experimental apparatus of synthesis of nanoparticles (a) and reactor used for N-alkylation reactions (b).

ature was kept at 70 °C for 4 min, then raised to 180 °C at 4 °C/min and maintained at this temperature for 1 min. Measurements performed up to 280 °C did not highlight the presence of other compounds (more weighted e.g. dialkylated amines, ...). The temperatures of the injector and detector were set at 250 °C and 250 °C, respectively. Helium was used as the carrier gas. The KBr technique was applied for determining the FT-IR spectra of the samples by using Vertex 70 apparatus (Bruker Corporation). Spectra were recorded in the scanning range from 4000 to 400 cm<sup>-1</sup>.

## 2. Results and Discussion

The two catalysts have been investigated by X-ray diffraction, thermal analysis, electron microscopy and FT-IR spectroscopic.

### 2.1 Characterization of the Nanocatalysts

#### 2.1.1 X-Ray Diffraction Analysis

X-ray diffraction patterns of both Fe<sub>3</sub>O<sub>4</sub>/AuSM and Fe<sub>3</sub>O<sub>4</sub>/AuCS nanocatalysts are shown in Figure 2. In the XRD spectrum of Fe<sub>3</sub>O<sub>4</sub>/AuSM, Figure 2a, the characteristic crystal planes well match with (111) at 18.5°, (220) at 30.4°, (311) at 35.4°, (400) at 43.2°, (422) at 53.7°, (511) at 57.4° and (440) at 62.7° of magnetite.<sup>[70,75–83]</sup> Scherrer's equation was used to measure the crystalline sizes, ~9 nm was found quite close to the TEM particles size measured, see below. It means that all the as-synthesized particles are single crystal. Lattice parameter "a"

and interplanar spacing  $d_{hkl}$ <sup>[77]</sup> were found to be  $a = 8.391 \text{ \AA}$  and  $d_{311} = 2.530 \text{ \AA}$ , they match with the standard lattice parameter of magnetite (8.396 Å) and are relatively far from the one of magnetite (8.346 Å), indicating that the as-synthesized iron oxide NPs are in magnetite phase.<sup>[82]</sup>

In the XRD pattern of the core-shell Fe<sub>3</sub>O<sub>4</sub>/AuCS, Figure 2b, the spectrum of Au shell prevails. It shows a strong diffraction peak at 38.5° attributed to (111) facet of the face-centered cubic metal gold structure. The other diffraction peaks (44.5°, 64.3°, 77.6° and 81.4°) the facets of (200), (220), (311) and (222) (JCPDS File number 04-0784) were also observed.

#### 2.1.2 Thermal Analysis

To estimate the thermal stability of both Fe<sub>3</sub>O<sub>4</sub>/AuSM and Fe<sub>3</sub>O<sub>4</sub>/AuCS nanocatalysts, thermogravimetric analysis was carried out. In Figure 3a and Figure 3b, the TG/DTG profiles, in the temperature range 25–900 °C, of Fe<sub>3</sub>O<sub>4</sub>/AuSM and Fe<sub>3</sub>O<sub>4</sub>/AuCS are shown, respectively. The first weight loss up to 180 °C, which is equal to ~3 wt.% for Fe<sub>3</sub>O<sub>4</sub>/AuSM and Fe<sub>3</sub>O<sub>4</sub>/AuCS, can be attributed to solvent release. In the range 200–400 °C, the weight loss, due to the oxidation/degradation of the organic oleic acid chains, which cover the NPs surface,<sup>[84–99]</sup> occurs. These weight loss account for ~16 wt.% and ~12 wt.% for Fe<sub>3</sub>O<sub>4</sub>/AuSM and Fe<sub>3</sub>O<sub>4</sub>/AuCS, respectively; indeed, the samples after washing show residual amounts of organic chains linked on the nanoparticles surface, lower in the case of the core-shell nanoparticles probably due to the NPs larger diameter.

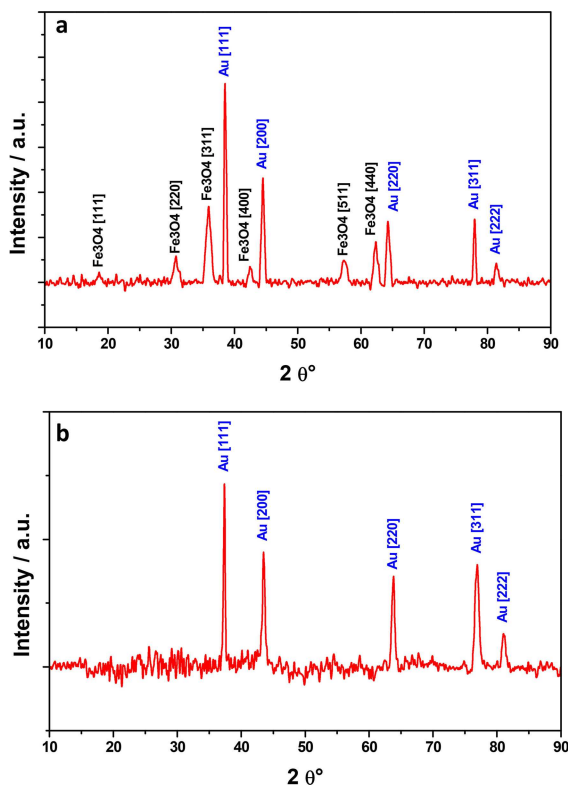


Figure 2. XRD spectra of Fe<sub>3</sub>O<sub>4</sub>/AuSM (a) and Fe<sub>3</sub>O<sub>4</sub>/AuCS (b).

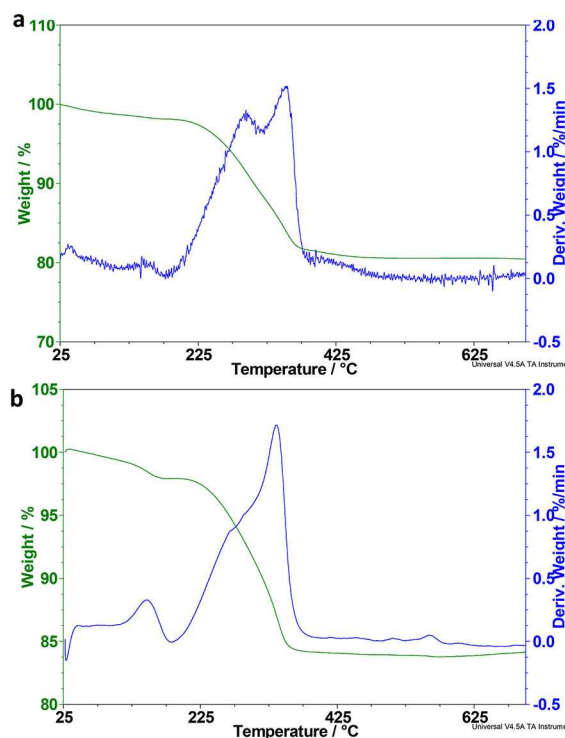
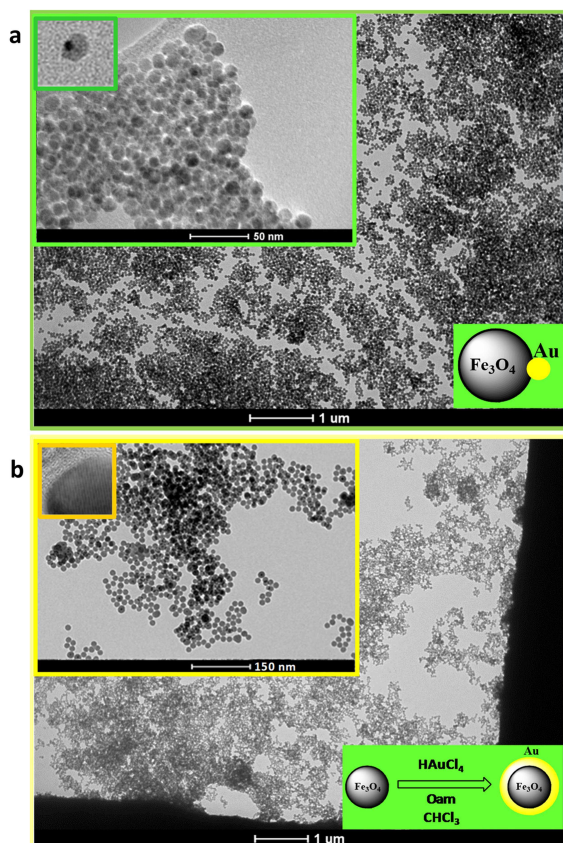


Figure 3. TG-DTG profiles of Fe<sub>3</sub>O<sub>4</sub>/AuSM (a) and Fe<sub>3</sub>O<sub>4</sub>/AuCS (b).



**Figure 4.** TEM images at different magnifications of  $\text{Fe}_3\text{O}_4/\text{AuSM}$  (a) and  $\text{Fe}_3\text{O}_4/\text{AuCS}$ .

### 2.1.3 Microscopic Analysis

The high resolution transmission electron microscopy (HR-TEM) images of both  $\text{Fe}_3\text{O}_4/\text{AuSM}$  and  $\text{Fe}_3\text{O}_4/\text{AuCS}$  NPs are shown in Figure 4. In particular, Figure 4a represents an HRTEM image of the snowman-like  $\text{Fe}_3\text{O}_4/\text{AuSM}$  NPs, that are characterized by a quasi-spherical  $\text{Fe}_3\text{O}_4$  NPs (about 9 nm diameter) supporting Au NPs ( $\sim 2$  nm diameter). Figure 4b shows the HRTEM image of the core-shell  $\text{Fe}_3\text{O}_4/\text{AuCS}$  nanocatalyst showing nanoparticles with an average diameter of  $\sim 10$  nm coated with a layer (of

$\sim 2.5$  nm) of crystalline Au. In the insert of Figure 4b, a HRTEM image of a single  $\text{Fe}_3\text{O}_4/\text{AuCS}$  NPs is shown. The lattice fringes in the Au shell are clearly seen in the image, the inter-fringe spacing is of 0.201 nm, close to the interplane distance of the (200) planes in the face centered cubic (fcc) Au, indicating that the  $\text{Fe}_3\text{O}_4$  nanoparticles are coated with a layer of crystalline Au. Au/Fe atomic ratios of  $\sim 0.032$  and of  $\sim 3.6$  were evaluated from energy dispersive TEM based x-ray spectroscopy (EDS) for  $\text{Fe}_3\text{O}_4/\text{AuSM}$  and  $\text{Fe}_3\text{O}_4/\text{AuCS}$  NPs, respectively. These values indicate a gold deposition yield of 64% and 75%, as gold absorption is not quantitative. On the other hand, the atomic ratio Fe/O results of 0.68 for  $\text{Fe}_3\text{O}_4/\text{AuSM}$  and of 0.71 for  $\text{Fe}_3\text{O}_4/\text{AuCS}$ , likely due to the oxygen from the organic chains.

## 2.2 Catalytic Activity

The catalytic performance of the magnetite/gold nanocatalysts were investigated for the N-alkylation of amines using benzyl alcohol as the source of alkyl group, toluene as solvent and under  $\text{N}_2$  atmosphere (Figure 5) in the experimental apparatus shown in Figure 1b.

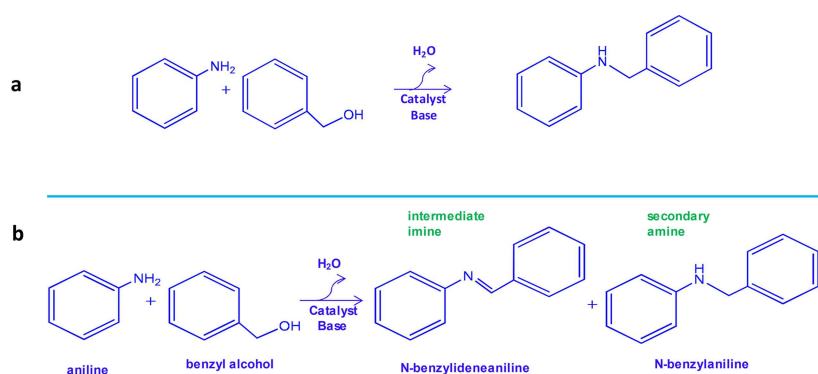
### 2.2.1 Catalytic N-Alkylation

The activity of the catalysts was tested for the N-alkylation of aniline using benzyl alcohol as alkylating agent. Firstly, we have optimized the reaction conditions in terms of base (see Table 1),

**Table 1.** Optimization of base and catalyst for the N-alkylation reaction of aniline with benzyl alcohol. Reaction conditions: aniline (1 mmol), benzyl alcohol (1 mmol), toluene (5 ml), catalyst (1 mg), base (2 mmol), temperature  $100^\circ\text{C}$ ,  $\text{N}_2$  flow, 4 h.

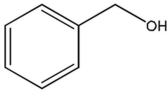
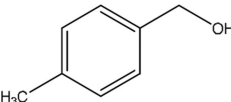
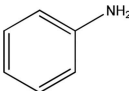
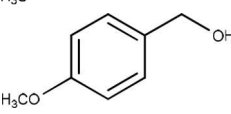
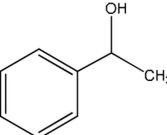
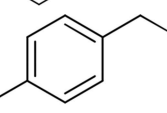
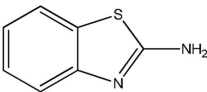
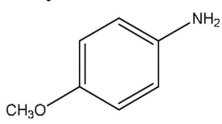
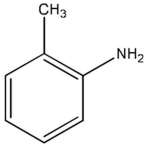
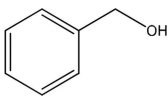
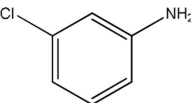
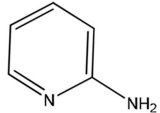
Entry	Catalyst	Base	Yield/%*
0	–	–	–
1	$\text{Fe}_3\text{O}_4/\text{AuSM}$	–	$9 \pm 1.4$
2	$\text{Fe}_3\text{O}_4/\text{AuSM}$	$\text{K}_2\text{CO}_3$	$23 \pm 0.9$
3	$\text{Fe}_3\text{O}_4/\text{AuSM}$	$\text{Cs}_2\text{CO}_3$	$34 \pm 0.5$
4	$\text{Fe}_3\text{O}_4/\text{AuCS}$	–	$24 \pm 1.3$
5	$\text{Fe}_3\text{O}_4/\text{AuCS}$	$\text{Cs}_2\text{CO}_3$	$> 99$

\* The Yield is referred to benzyaniline formation



**Figure 5.** Schemes of N-alkylation reaction of: aniline with benzyl alcohol (a); example of a possible reaction pathway, with both the intermediate imine and secondary amine formation, from aniline (b).

**Table 2.** Effect of gold on the N-alkylation. Reaction conditions: aniline (1 mmol), benzyl alcohol (1 mmol), toluene (5 ml), catalyst (1 mg), Cs<sub>2</sub>CO<sub>3</sub> (2 mmol), temperature 100 °C, N<sub>2</sub> flow, 4 h.

Entry	R <sub>1</sub> NH <sub>2</sub>	R <sub>2</sub> OH	Reaction		Yield/% <sup>a</sup> Fe <sub>3</sub> O <sub>4</sub> /AuSM	Yield/% <sup>a</sup> Fe <sub>3</sub> O <sub>4</sub> /AuCS
			$R_1-NH_2 + R_2-OH \xrightarrow[\text{Toluene; Catalyst}]{Cs_2CO_3}$	$R_1-NH-R_2$		
1					34 ± 0.5	> 99
2					37 ± 1.2	97 ± 0.5
3					39 ± 1.1	98 ± 0.7
4					27 ± 1.2	90 ± 0.8
5					24 ± 1.3	88 ± 0.9
6					32 ± 1.2	99 ± 0.8
7					34 ± 1.4	> 99
8					31 ± 1.1	> 99
9					27 ± 1.3	89 ± 0.6
10					26 ± 0.9	94 ± 1.6

<sup>a</sup>Reaction conditions: amine (1 mmol), alcohol (1 mmol), toluene (5 ml), catalyst (1 mg), Cs<sub>2</sub>CO<sub>3</sub> (2 mmol), temperature 100 °C, N<sub>2</sub> flow, 4 h.

then, we performed the reaction in the absence of any catalyst in order to prove its real effect (Table 2).<sup>[100–104]</sup> The addition of a Cs<sub>2</sub>CO<sub>3</sub> base promoter, led to a significant increase of the yield up to a value higher than 99% (Table 1, entries 4 and 5). On the other hand, benzyl alcohol and aniline did not form any products in the absence of a catalyst, see Figure S2 and Table 1 entry 0.

The N-alkylation of the amines using alcohols were analyzed through a GC-MS. In particular, GC-MS spectra of the reaction

mixture in N-alkylation of aniline with benzyl alcohol at different time using snowman-like Fe<sub>3</sub>O<sub>4</sub>/AuSM NPs are shown in Figure 6. At the beginning of the reaction (t = 0 h) the dominant peaks due to the solvent are visible. Minor peaks due to aniline and benzyl alcohol are also present. After 1 h reaction, an aniline conversion of about 17% was achieved with N-benzylideneaniline as the dominant product (signal at 30.7 min), the desired N-benzylaniline is not yet visible. After 4 h reaction, an aniline conversion of about 57% was achieved,

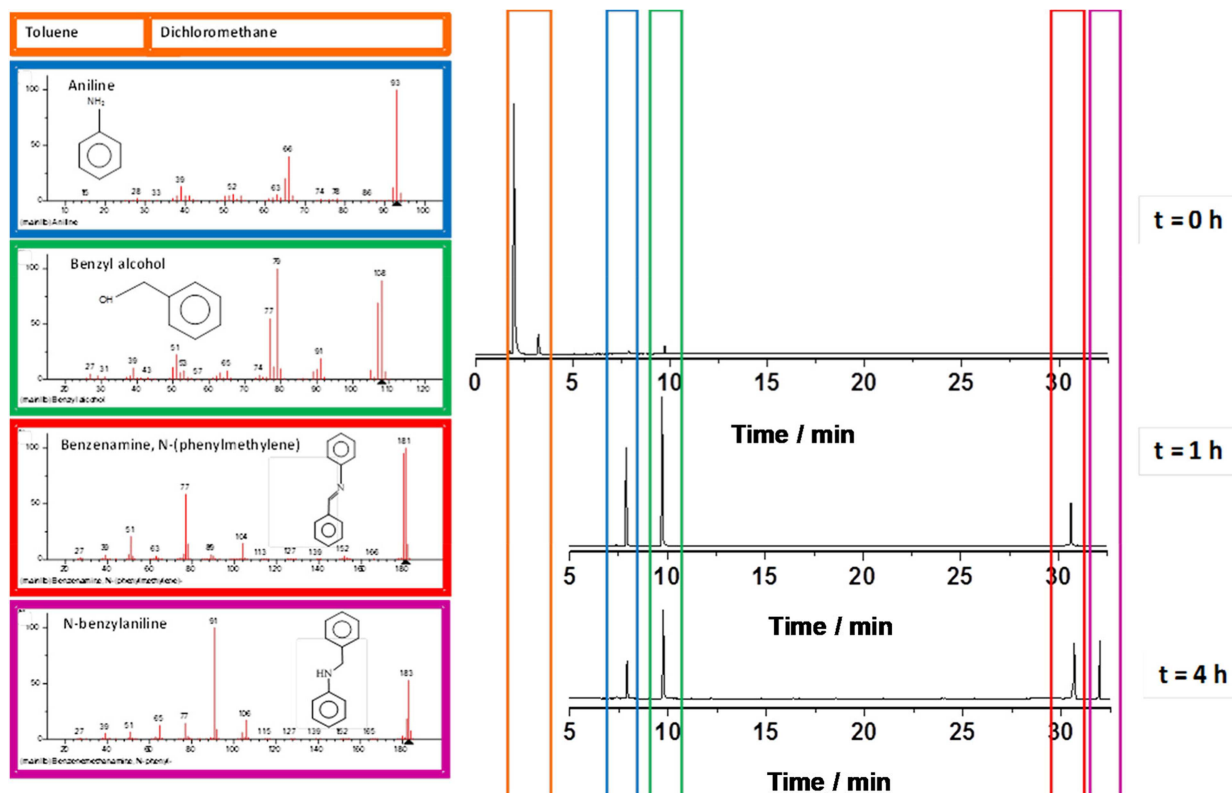


**Figure 6.** GC spectra of reaction mixture in N-alkylation of aniline with benzyl alcohol at different time using snowman like  $\text{Fe}_3\text{O}_4/\text{AuSM}$  NPs. Reaction conditions: aniline (1 mmol), benzyl alcohol (1 mmol), toluene (5 ml),  $\text{Fe}_3\text{O}_4/\text{AuSM}$  (1 mg),  $\text{Cs}_2\text{CO}_3$  (2 mmol), temperature  $100^\circ\text{C}$ ,  $\text{N}_2$  flow. Pretreatment on anhydrous  $\text{Na}_2\text{SO}_4$  and dried under vacuum. For the GC: maximum temperature of  $180^\circ\text{C}$ .

with the intermediate imine N-benzylideneaniline product (signal at 30.7 min) and the desired N-benzylaniline (signal at 32.0 min) as the major product (yield of  $34\% \pm 0.5$ ). With  $\text{Fe}_3\text{O}_4/\text{AuSM}$  NPs catalyst a conversion higher than 90% with a N-benzylaniline, yield of about 54%, was achieved after 24 h, which undergoes very small variations in the following hours. In Figure 7, GC-MS spectra of the reaction mixture in N-alkylation of aniline using benzyl alcohol as the alkylating agent and core-shell  $\text{Fe}_3\text{O}_4/\text{AuCS}$  NPs nanocatalyst, at different times, are shown. Also in this case, at the beginning of the reaction ( $t = 0$  h), dominant peaks, in the first minutes, due to solvent are visible. Minor peaks due to aniline and benzyl alcohol are also present. After 1 h reaction, an aniline conversion of about 43% was achieved with N-benzylaniline as the dominant product (signal at 32.0 min). After, only, 4 h reaction under flowing  $\text{N}_2$ , an almost complete conversion of aniline was achieved. The concentration of the intermediate N-benzylideneaniline was now fallen to  $\sim 0\%$ , whereas the desired N-benzylaniline was formed with  $> 99\%$  yield.

We have also explored the catalytic efficiency of the  $\text{Fe}_3\text{O}_4/\text{AuSM}$  and  $\text{Fe}_3\text{O}_4/\text{AuCS}$  as nanocatalysts in N-alkylation of aniline and benzyl alcohol using  $\text{Cs}_2\text{CO}_3$  in presence of different substrates.

The N-alkylation of aniline with different alcohol is shown in Table 2 entry 1–10. When aniline was reacted with Ph–Me and Ph–MeO substituted benzyl alcohols (Table 2, entry 2 and entry 3) good yields, of  $\sim 97\%$  and  $\sim 98\%$ , respectively, are

achieved. On other hand, secondary alcohols are challenging alkylating agents compared with primary alcohols because of the dehydrogenation of secondary alcohols to the corresponding ketones is more difficult than that of primary alcohols (Table 2 entry 4).<sup>[105]</sup> When benzyl alcohol substituted electron-withdrawing -Cl group reacts with aniline the alkylation results more slowly than with primary alcohols (Table 2 entry 5). It was observed that the rate of reaction in the presence of electron donating groups, like methyl or methoxy (entry 7 and 8), was faster than with milder electron withdrawing groups like halogens (Table 2, entries 9).<sup>[50,106]</sup>

The 2-aminobenzothiazole and 2-aminopyridine N-alkylation were also analyzed using  $\text{Cs}_2\text{CO}_3$  as promoter in toluene, see Table 2 (entry 6 and 10). Yield of about 99% was achieved in the N-alkylation of 2-aminobenzothiazole, whereas yield of 94% was obtained in the N-alkylation of the 2-aminopyridine molecule because of its different electrophile behavior.<sup>[50,57]</sup>

As far as N-alkylation of aniline, using alcohols as alkylating agent, is concerned, see Table 3, it is evident that high activity and fast kinetic can be achieved, requiring, especially in the case of heterogeneous catalysis, temperatures higher than  $140^\circ\text{C}$ .<sup>[26,32–39,43,46,50–59]</sup> The high conversion achieved in short time by small amount of our nanoparticles, that can be easily separated thanks to the magnetic component, suggests a catalytic behavior approaching homogeneous catalysis.

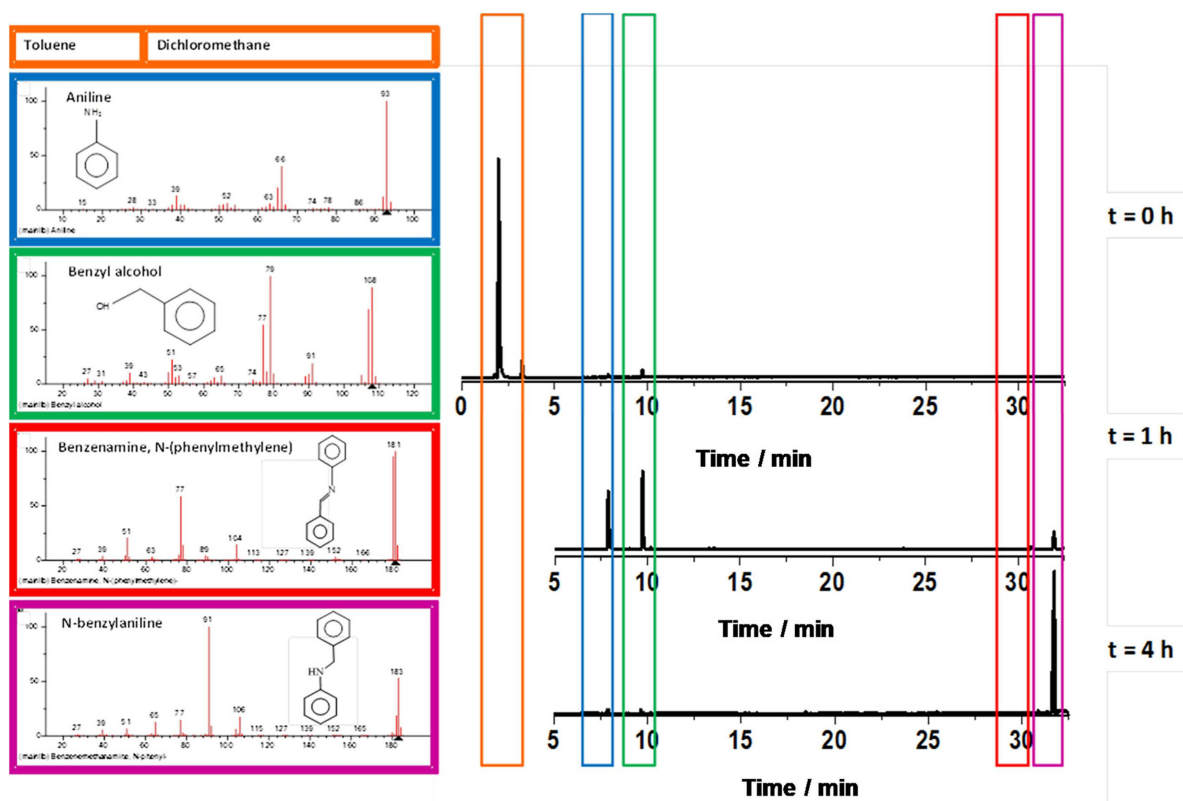


**Figure 7.** GC spectra of reaction mixture in N-alkylation of aniline with benzyl alcohol at different time using core-shell  $\text{Fe}_3\text{O}_4/\text{AuCS}$  NPs. Reaction conditions: aniline (1 mmol), benzyl alcohol (1 mmol), toluene (5 ml),  $\text{Fe}_3\text{O}_4/\text{AuCS}$  (1 mg),  $\text{Cs}_2\text{CO}_3$  (2 mmol), temperature  $100^\circ\text{C}$ ,  $\text{N}_2$  flow. Pretreatment on anhydrous  $\text{Na}_2\text{SO}_4$  and dried under vacuum. For the GC: maximum temperature of  $180^\circ\text{C}$ .

### 2.2.2 FT-IR Spectroscopic Studies

In particular, in the  $\text{Fe}_3\text{O}_4/\text{AuCS}@OA$  spectrum (Figure 8a), typical peaks at  $637$  and  $590\text{ cm}^{-1}$  are present due to the bonds  $\nu_1(\text{Fe}-\text{O})$  and  $\nu_2(\text{Fe}-\text{O})$ .<sup>[107]</sup> In the IR spectrum of the  $\text{Fe}_3\text{O}_4/\text{AuCS}@OA$ , the presence of oleic acid as a capping agent on the surface is confirmed by the peaks at  $1540\text{ cm}^{-1}$  and  $1660\text{ cm}^{-1}$ , due to the asymmetric  $\nu_{\text{as}}(\text{COO}^-)$  and the symmetric  $\nu_{\text{s}}(\text{COO}^-)$  stretch, indicating the bonding of the carboxylic acids on the nanoparticles surface.<sup>[70]</sup> On the other hand, no peaks from free carboxyl groups can be observed. The characteristic peaks of the oleic groups in the  $2850\text{--}3000\text{ cm}^{-1}$  region can be also seen.

The FT-IR spectrum of the reaction mixture after catalyst separation through a magnetic field and an hour of reaction using  $\text{Fe}_3\text{O}_4/\text{AuCS}@OA$  N-alkylation nanocatalyst, see Figure 8b, shows the typical peaks of N-benzylaniline C–H bending at  $692\text{ cm}^{-1}$  and  $750\text{ cm}^{-1}$ . The C–C stretching and  $\text{NH}_2$  scissoring of N-benzylaniline are visible at  $1507\text{ cm}^{-1}$  and  $1602\text{ cm}^{-1}$ . Bands due to C–N stretching can be seen in the range  $1000\text{--}1400\text{ cm}^{-1}$ . The band at  $3419\text{ cm}^{-1}$  can be assigned to the N–H stretching of N-benzylaniline, while the vibrational band at  $1727\text{ cm}^{-1}$  suggest the presence of free oleic acid in the reaction medium, likely evidencing that the reactive process was analyzed at an intermediate state. The bands at wavelenght close to  $3000\text{ cm}^{-1}$  can be attributed to C–H stretching coming

from the organic molecules present into the analyzed mixture. Very weak bands from N-benzylideneaniline, e.g at  $649\text{ cm}^{-1}$  and  $762\text{ cm}^{-1}$ , can be also detected. On the other hand, the spectrum of aniline (bands indicated by the blue arrows in the Figure 8b) is practically superimposable to that of N-benzylaniline, making difficult through FT-IR the identification of the two species, as evaluated by GC-MS, also due to the broadening of many bands that, indeed, suggests their contemporaneous presence.

The spectrum of N-benzylaniline recorded at 4 h, which is more resolved after 4 h (Figure 8c) suggests the almost complete conversion of the reagent in N-benzylaniline.

### 2.2.3 Recyclability of the Nanocatalysts

We have studied the recyclability of both nanocatalysts for the N-alkylation of aniline, 2-aminobenzothiazole and 2-aminopyridine, using benzyl alcohol as alkylating agent. The nanocatalysts can be easily recovered from the reaction medium just applying an external magnetic field, and then washed with distilled water and acetone. It was then dried and used for new runs. As we can see from Figure 9, the nanocatalysts can be successfully recycled ten times without any appreciable loss in the catalytic activity. This is likely due to the efficiency of the magnetic separation process. The weak decrease in product

Table 3. Literature survey of N-alkylation of amine with alcohols.

Catalyst	catalyst/solvent/ mg/ml per 1 mmol of amine	catalyst /mmol	Reaction Temperature/°C	Time /h	Base/ ligand or other	Conversion /%	Selectivity /%	Yield /%	Alcohol/amine	Ref.
Ru complex	5.05	0.025	110	24	K <sub>2</sub> CO <sub>3</sub> /li- gand	100	–	–	Phenethyl alcohol/ tert-butylamine	[26]
Co Complex	2.54	0.01	~ 100	48	ligand	–	up to 99	98	Benzyl alcohol/aniline	[32]
PdCl <sub>2</sub>	0.355	0.02	100	15	base/li- gand	100	–	96	Benzyl alcohol/aniline	[33]
[Cp*IrCl <sub>2</sub> ] <sub>2</sub>	0.192	0.005	110	17	NaHCO <sub>3</sub>	–	–	94	Benzyl alcohol/aniline	[34]
Ru complex	–	0.04	65	48	ligand	> 99	75	74	Benzyl alcohol/aniline	[36]
NiBr <sub>2</sub>	8.92	0.025	130	48	BuOK/li- gand	99	–	96	Benzyl alcohol/aniline	[37]
Ir complexes	0.54	0.03	110	5	KOT-Bu	99	–	–	Benzyl alcohol/aniline	[38]
Ir complexes	0.3 mol% in 0.3 ml toluene	0.003	100	4	ligand	99	–	–	Benzyl alcohol/aniline	[39]
Mn pincer complexes	3 mol% in 2 ml toluene	0.01	80	24	t-BuOK	91	–	78	Benzyl alcohol/aniline	[40]
NaOH	–	1	220	6	NaOH	99.6	99.5	–	Benzyl alcohol/aniline	[35]
Pd/Fe <sub>2</sub> O <sub>3</sub>	(Pd 2.28 wt.%)	0.15	160	2	–	100	94	90	Benzyl alcohol/aniline	[22]
Au/ZrO	–	1.5 mol% of Au	110	22	–	–	94	80	Benzyl alcohol/aniline	[42]
Au/Al-MIL53	24.7 (Au 2.5 wt.%)	0.18	110	22	Cs <sub>2</sub> CO <sub>3</sub>	–	–	16	Benzyl alcohol/aniline	[45]
Au/Al-MIL53	24.7 (Au 2.5 wt.%)	0.18	130	48	Cs <sub>2</sub> CO <sub>3</sub>	–	–	48	Benzyl alcohol/aniline	[45]
Ag/Al <sub>2</sub> O <sub>3</sub>	22 (Ag 2.4 wt.%)	0.309	120	19	Cs <sub>2</sub> CO <sub>3</sub>	> 99	> 99	> 99	Benzyl alcohol/aniline	[46]
Ag@Al <sub>2</sub> O <sub>3</sub>	4 (Ag 1.5 wt.%)	0.095	100	10	Cs <sub>2</sub> CO <sub>3</sub>	99	–	96	Benzyl alcohol/aniline	[49]
Pd/MgO	0.8 (Pd 0.8 wt.%)	0.680	180	0.25	–	99	–	79	Benzyl alcohol/aniline	[50]
Ni/(t-Al <sub>2</sub> O <sub>3</sub> ) <sup>a</sup>	8 (Ni 5 wt.%)	0.01	144	3	–	100	–	99	Benzyl alcohol/aniline	[51]
Cu- AcTp@Am-Si- Fe <sub>3</sub> O <sub>4</sub> <sup>b</sup>	0.8 (Cu 0.8 wt.%)	–	100	10	KOH	98	100	–	Benzyl alcohol/aniline	[52]
Al-MCM-41 <sup>c</sup>	–	–	300-400	–	–	Total	> 70	–	Methanol/aniline	[53]
Pd(AIO(OH))	17 (Pd 3.5 wt.%)	0.02	90	18	–	–	–	84	Benzyl alcohol/2-phe- nylethylamine	[54]
CuO	0.8	0.03	110	12	K <sub>2</sub> CO <sub>3</sub>	–	–	88	Benzyl alcohol/aniline	[55]
Au/TiO <sub>2</sub> -VS	1.3 (Au 1.2 wt.%)	0.5 mol% of Au	120	14	Cs <sub>2</sub> CO <sub>3</sub>	> 99	–	92	Benzyl alcohol/aniline	[56]
Au/TiO <sub>2</sub> -VS	4787 (Au 0.02 wt.%)	0.0083 mol % of Au	180	96	solvent free	> 99	–	98	Benzyl alcohol/aniline	[56]
Fe <sub>3</sub> O <sub>4</sub>	18.6	0.040	90	168	(CH <sub>3</sub> ) <sub>3</sub> COK	–	–	88	Benzyl alcohol/aniline	[57]
Fe-HMS <sup>d</sup>	10 (Fe 0.39 wt.%)	–	150-170	1.5	DABCO base	99	90	–	Benzyl alcohol/aniline	[58]
Fe <sub>3</sub> O <sub>4</sub> @Au	0.2	0.005	100	4	Cs <sub>2</sub> CO <sub>3</sub>	> 99	–	> 99	Benzyl alcohol/aniline	This work

<sup>a</sup> pre-reduced at 500 °C under a flow of H<sub>2</sub> for 0.5 h; <sup>b</sup> aerobic N-alkylation; <sup>c</sup> tubular stainless steel, continuous flow mixed-bed microreactor; <sup>d</sup> microwave irradiation (300 W max. power output); <sup>e</sup> air atmosphere.

yield could be attributed to a small loss of the catalyst during the recycling process and a weak reduction of the catalytic activity due to uses.

### 2.2.4 Reaction Mechanism

A possible reaction pathway, taking the reaction shown in Figure 5 as a model, is presented in Figure 10.

First of all, in order to confirm the reaction mechanism, an experiment was performed under an excess of benzyl-alcohol (molar ratio benzyl-alcohol/aniline equal to 3:1.5) and by using Fe<sub>3</sub>O<sub>4</sub>/AuCS@OA or Fe<sub>3</sub>O<sub>4</sub>/AuSM@OA as catalyst, which allowed to observe the formation of the relative aldehyde (GC-MS evaluated, retention time 8.4 min, after 4 h), together with small amount of benzyl benzoate (retention time 34.7 min), suggest-

ing that a borrowing hydrogen is active in the process.<sup>[108]</sup> The contribution of the base during the dehydrogenation step to form the alkoxide is evident, see Table 1. Indeed, the base helps the Lewis acid behavior of the surface in the deprotonation of the alcohol,<sup>[59]</sup> since the reaction proceeds slowly without base. We believe that the reaction proceeds with the transitory formation of catalyst surface hydride species (Schemes in Figure 10 for a possible reaction mechanism and Figure S1 for FT-IR spectrum of the Fe<sub>3</sub>O<sub>4</sub>/AuCS@OA NPs after 1 h reaction). To establish that the process involves the formation of the hydride, an additional experiment was performed in the absence of amine. The mixture after 1 h of reaction in presence of Fe<sub>3</sub>O<sub>4</sub>/AuCS@OA was analyzed by FT-IR. The intermediate formation of Au–H species in the FT-IR spectral range of 2125–2130, peak at about 2132 cm<sup>–1</sup>,<sup>[109,110]</sup> can be observed, see Figure S1. Although, the peak is weak, it can be assigned to the



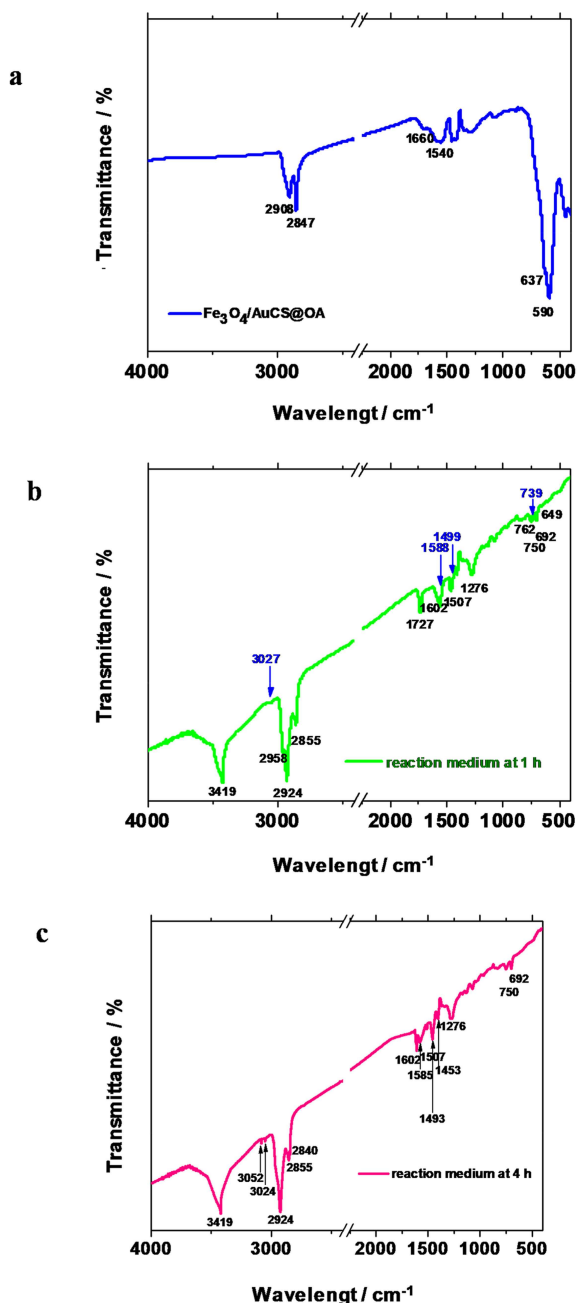


Figure 8. FT-IR spectra in the range 4000–500  $\text{cm}^{-1}$  of:  $\text{Fe}_3\text{O}_4/\text{AuCS}@OA$  NPs (a); reaction medium at 1 h (b); reaction medium at 4 h (c).

presence of gold-hydride intermediated species. Similarly to what happens in homogeneous catalysis, a role of the ligand chains of OA, forming complexes with the nanoparticles surface, cannot be neglected. A cooperative mechanism due to generation of coordinative functionality, similar to unsaturated metal centers, followed by a simultaneous carboxylic protonation (see the previous FT-IR analysis paragraph), which helps the continuous base regeneration, probably occurs.

A scheme of the possible reaction pathway is shown in Figure 10 c. The removal of a hydrogen from the alkoxide (A), to form hydride with the catalyst surface, leads to the formation of the carbonyl compound (B). The carbonyl compound quickly

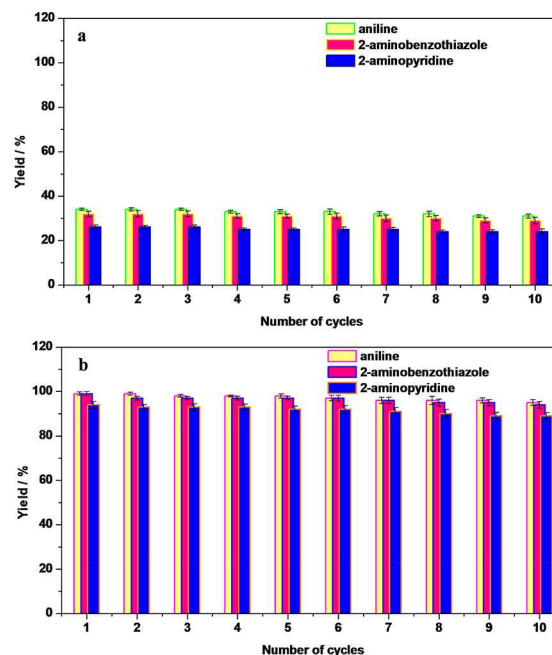
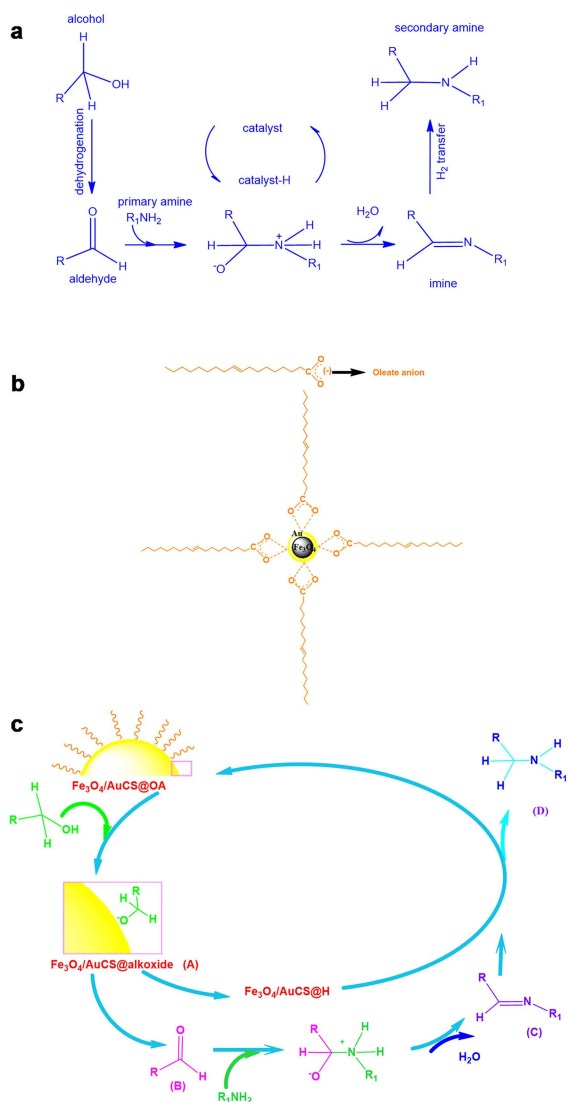


Figure 9. Recycling efficiency of  $\text{Fe}_3\text{O}_4/\text{AuSM}$  (a) and of  $\text{Fe}_3\text{O}_4/\text{AuCS}$  (b) in the N-alkylation of amines.

reacts with a primary amine to form the corresponding imine (C). Finally, it is then reduced by the catalyst, hydrogen is then transferred back to the imine to yield the corresponding secondary amine (D) and restituting the catalyst OA complex.

Although, in the two catalysts, the components are the same, i.e. magnetite and gold, the catalysts morphologies and exposed surfaces are different. The high activity and selectivity showed by the catalysts can be ascribed to the small dimensions, high surface area, absence of diffusion limitation and homogeneous dispersion, together with the surface properties and the presence of the base. In particular, during the amine formation the small size of the Au NPs<sup>[51,111]</sup> and electron transfer through the Au NPs to the imine favor the subsequent hydrogen transfer.<sup>[112]</sup> The kinetic of the snowman-like catalyst, which results better than that shown by magnetite alone,<sup>[58]</sup> can be attributed to the nanosize of the catalyst, the cooperative mechanism between base and surfactant inducing additional surface coordinative functionality, and to the hetero-junction between the different work-function of the Au and magnetite components, which allows electron flow from the  $\text{Fe}_3\text{O}_4$  to Au enhancing the Lewis acid behavior of the  $\text{Fe}_3\text{O}_4$  surface. On the other hand, the catalyst at the same time shows a lower selectivity. Moreover, core-shell NPs, exposing a gold surface to the reaction medium, show higher selectivity to amine<sup>[113]</sup> in the a-polar solvent used, and this is because of their more pronounced nucleophile nature, influencing the selectivity and thus activity of the catalyst. An additional experiment performed with gold alone led to a yield reduction (40% reduction after 4 h), confirming the role of magnetite core in enhancing surface electron donating behavior. This is because the rate limiting step in the formation of the amine from imine was the hydride transfer via metal-hydride inter-



**Figure 10.** Schemes of possible hydrogen autotransfer process from alcohol to amine (a, b, c).

mediates (borrowing hydrogen)<sup>[51,57,114,115]</sup> to reduce imine, which increases the selectivity of the process<sup>[43]</sup> and, at the same time, releases the active sites of the catalyst.

### 3. Conclusion

Two new nanocatalysts, based on gold and magnetite, stable in reaction media and easily recoverable and recyclable were designed and tested for N-alkylation of amines using alcohols. HRTEM images of the snowman-like Fe<sub>3</sub>O<sub>4</sub>/AuSM NPs show that they are characterized by a quasi-spherical Fe<sub>3</sub>O<sub>4</sub> NPs (about 9 nm diameter) supporting Au NPs (~2 nm diameter). Fe<sub>3</sub>O<sub>4</sub>/AuCS core-shell NPs are constituted of nanoparticles with an average diameter of ~10 nm coated with a layer of ~2.5 nm of crystalline Au.

Benzyl alcohol and aniline did not form any products in the absence of catalyst. The surface behavior of nanoparticle and

the addition of a Cs<sub>2</sub>CO<sub>3</sub> base promoter are fundamental to obtain yields up to a value higher than >99% in toluene. The high activity and selectivity showed by the catalysts can be ascribed to: small dimensions; high surface area; absence of diffusion limitation and homogeneous dispersion; a ligands cooperation mechanism, due to generation of unsaturation on metal surface in the presence of the base. Core-shell NPs show higher activity because of their more pronounced nucleophile nature, influencing the activity and selectivity of the catalyst. Indeed, the rate limiting step in the formation of the amine from imine was the hydride transfer via metal-hydride intermediates (borrowing hydrogen) to reduce imine, which increases the selectivity of the process] releasing the catalyst active sites.

The nanocatalysts can be easily recovered from the reaction medium just applying an external magnetic field and successfully recycled ten times without any appreciable loss in the catalytic activity, likely due to the efficiency of the magnetic separation process. It is worth noticing, that the method for N-alkylation chosen is atom-economic and environmental friendly, as alcohols are abundant and water is the only by-product. This paper is, also, a proof of concept of the possibility to use new nanocatalyst synthesis approaches, based on the combination of self-dispersible active species and magnetic components, for a catalysis between homogeneous and heterogeneous.

### Conflict of Interest

The authors declare no conflict of interest.

**Keywords:** N-alkylation · borrowing hydrogen · nanocatalysis · high selectivity processes · green chemistry

- [1] S. A. Lawrence, *Amines: Synthesis, Properties and Application*, Cambridge University, Cambridge, **2004**.
- [2] T. Mizuta, S. Sakaguchi, Y. J. Ishii, *Org. Chem.* **2005**, *70*, 2195–2199.
- [3] T. E. Müller, K. C. Hultsch, M. Yus, F. Foubelo, M. Tada, *Chem. Rev.* **2008**, *108*, 3795–3892.
- [4] T. C. Nugent, M. El-Shazly, *Adv. Synth. Catal.* **2010**, *352*, 753–819.
- [5] K. Krüger, A. Tillack, M. Beller, *ChemSusChem.* **2009**, *2*, 715–717.
- [6] J. Ward, R. Wohlgemuth, *Curr. Org. Chem.* **2010**, *14*, 1914–1927.
- [7] D. Crozet, M. Urrutigoity, P. Kalck, *ChemCatChem* **2011**, *3*, 1102–1118.
- [8] R. Grigg, T. R. B. Mitchell, S. Sutthivaiyakit, N. Tongpenyai, *J. Chem. Soc. Chem. Commun.* **1981**, *0*, 611–612.
- [9] Y. Watanabe, Y. Tsuji, H. Ige, Y. Ohsugi, T. Ohta, *J. Org. Chem.* **1984**, *49*, 3359–3363.
- [10] G. Guillena, D. J. Ramón, M. Yus, *Chem. Rev.* **2010**, *110*, 1611–1641.
- [11] G. E. Dobreiner, R. H. Crabtree, *Chem. Rev.* **2010**, *110*, 681–703.
- [12] T. D. Nixon, M. K. Whittlesey, J. M. J. Williams, *Dalton Trans.* **2009**, *0*, 753–762.
- [13] G. W. Lamb, J. M. J. Williams, *Chim. Oggi-Chem. Today* **2008**, *26*, 17–19.
- [14] M. H. S. A. Hamid, P. A. Slatford, J. M. J. Williams, *Adv. Synth. Catal.* **2007**, *349*, 1555–1575.
- [15] G. Guillena, D. J. Ramón, M. Yus, *Angew. Chem.* **2007**, *119*, 2410–2416; *Angew. Chem. Int. Ed.* **2007**, *46*, 2358–2364.
- [16] Audrey Moores in *Homogeneous Catalysis* (Ed.: Robert H. Crabtree) a Volume of the Green Chemistry Series, Ed. Paul Anastas, Wiley-VCH, **2009**, 1–15.
- [17] B. M. Trost, *Angew. Chem.* **1995**, *107*, 285–307; *Angew. Chem. Int. Ed. Engl.* **1995**, *34*, 259–281.
- [18] K. I. Fujita, R. Yamaguchi, *Synlett* **2005**, 560–571.

- [19] T. Suzuki, *Chem. Rev.* **2011**, *111*, 1825–1845.
- [20] S. Bähn, S. Imm, L. Neubert, M. Zhang, H. Neumann, M. Beller, *ChemCatChem* **2011**, *3*, 1853–1864.
- [21] M. H. S. A. Hamid, C. L. Allen, A. C. Maxwell, H. C. Maytum, A. J. A. Watson, J. M. J. Williams, *J. Am. Chem. Soc.* **2009**, *131*, 1766–1774.
- [22] Y. Zhang, X. Qi, X. Cui, F. Shi, Y. Deng, *Tetrahedron Lett.* **2011**, *52*, 1334–1338.
- [23] F. Li, H. Shan, Q. Kang, L. Chen, *Chem. Commun.* **2011**, *47*, 5058–5060.
- [24] F. Li, H. Shan, L. Chen, Q. Kang, P. Zou, *Chem. Commun.* **2012**, *48*, 603–605.
- [25] F. Li, L. Chen, Q. Kang, J. Cai, G. Zhu, *New J. Chem.* **2013**, *37*, 624–631.
- [26] M. Haniti, S. A. Hamid, J. M. J. Williams, *Chem. Commun.* **2007**, *0*, 725–727.
- [27] M. Haniti, S. A. Hamid, J. M. J. Williams, *Tetrahedron Lett.* **2007**, *48*, 8263–8265.
- [28] K. Fujita, Z. Li, N. Ozeki, R. Yamaguchi, *Tetrahedron Lett.* **2003**, *44*, 2687–2690.
- [29] A. Prades, R. Corberan, M. Poyatos, E. Peris, *Chem. Eur. J.* **2008**, *14*, 11474–11479.
- [30] F. Shi, M. K. Tse, X. Cui, D. Gördes, D. Michalik, K. Thurow, Y. Deng, M. Beller, *Angew. Chem. Int. Ed.* **2009**, *48*, 5912–5915.
- [31] Y. Q. Wang, S. M. Lu, Y. G. Zhou, *J. Org. Chem.* **2007**, *72*, 3729–3734.
- [32] G. Zhang, Z. Yin, S. Zheng, *Org. Lett.* **2016**, *18*, 300–303.
- [33] T. T. Dang, B. Ramalingam, S. P. Shan, A. M. Seayad, *ACS Catal.* **2013**, *3*, 2536–2540.
- [34] K. Fujita, Y. Enoki, R. Yamaguchi, *Tetrahedron* **2008**, *64*, 1943–1954.
- [35] X. H. Lu, Y. W. Sun, X. L. Wei, C. Peng, D. Zhou, Q. H. Xia, *Catal. Commun.* **2014**, *55*, 78–82.
- [36] A. B. Enyong, B. Moasser, *J. Org. Chem.* **2014**, *79*, 7553–7563.
- [37] M. Vellakkaran, K. Singh, D. Banerjee, *ACS Catal.* **2017**, *7*, 8152–8158.
- [38] M. V. Jiménez, J. Fernández-Tornos, M. González-Lainez, B. Sánchez-Page, F. J. Modrego, L. A. Oro, J. J. Pérez-Torrente, *Catal. Sci. Technol.* **2018**, *8*, 2381–2393.
- [39] P. Dubey, S. Gupta, A. K. Singh, *Dalton Trans.* **2018**, *47*, 3764–3774.
- [40] S. Elangovan, J. Neumann, J. B. Sortais, K. Junge, C. Darcel, M. Beller, *Nat. Commun.* **2016**, *7*, 12641.
- [41] O. Saidi, A. J. Blacker, M. M. Farah, S. P. Marsden, J. M. J. Williams, *Angew. Chem. Int. Ed.* **2009**, *121*, 7511–7514.
- [42] G. Reyes-Rios, J. J. García, *Inorg. Chim. Acta* **2012**, *392*, 317–321.
- [43] T. Ishida, R. Takamura, T. Takei, T. Akita, M. Haruta, *Appl. Catal. A* **2012**, *413–414*, 261–266.
- [44] O. Takashi, M. Yoshiki, I. Junji, N. Yasuhito, U. Masaru, M. Kazushi, *J. Am. Chem. Soc.* **2009**, *131*, 14317–14328.
- [45] J. W. Kim, K. Yamaguchi, N. Mizuno, *J. Catal.* **2009**, *263*, 205–208.
- [46] T. Ishida, N. Kawakita, T. Akita, M. Haruta, *Gold Bull.* **2009**, *42*, 267–274.
- [47] H. Liu, G.-K. Chuah, S. Jaenicke, *J. Catal.* **2012**, *292*, 130–137.
- [48] U. Mandi, S. K. Kundu, N. Salam, A. Bhaumik, S. M. Islam, *J. Colloid Interface Sci.* **2016**, *467*, 291–299.
- [49] Q. Xu, Q. Li, X. G. Zhu, J. H. Chen, *Adv. Synth. Catal.* **2013**, *355*, 73–80.
- [50] P. Paul, P. Bhanja, N. Salam, U. Mandi, A. Bhaumik, S. M. Alam, Sk. M. Islam, *J. Colloid Interface Sci.* **2017**, *493*, 206–217.
- [51] A. Corma, T. Ródenas, M. J. Sabater, *Chem. Eur. J.* **2010**, *16*, 254–260.
- [52] K. Shimizu, N. Imaida, K. Kon, S. M. A. H. Siddiki, A. Satsuma, *ACS Catal.* **2013**, *3*, 998–1005.
- [53] R. K. Sharma, Y. Monga, A. Puri, G. Gaba, *Green Chem.* **2013**, *15*, 2800–2809.
- [54] R. Luque, J. M. Campelo, D. Luna, J. M. Marinas, A. A. Romero, *J. Mol. Catal. A*, **2007**, *269*, 190–196.
- [55] M. S. Kwon, S. Kim, S. Park, W. Bosco, R. K. Chidrala, J. Park, *J. Org. Chem.* **2009**, *74*, 2877–2879.
- [56] N. Mittapelly, B. R. Reguri, K. Mukkanti, *Der Pharma Chem.* **2011**, *3*, 180–189.
- [57] L. He, X. B. Lou, J. Ni, Y. M. Liu, Y. Cao, H. Y. He, K. N. Fan, *Chem. Eur. J.* **2010**, *16*, 13965–13969.
- [58] R. Martínez, D. J. Ramón, M. Yus, *Org. Biomol. Chem.* **2009**, *7*, 2176–2181.
- [59] C. Gonzalez-Arellano, K. Yoshida, R. Luque, P. L. Gai, *Green Chem.* **2010**, *12*, 1281–1287.
- [60] H. Althues, J. Henle, S. Kaskel, *Chem. Soc. Rev.* **2007**, *36*, 1454–1465.
- [61] Z. W. Li, Y. F. Zhu, *Appl. Surf. Sci.* **2003**, *211*, 315–320.
- [62] M. Jafarpour, M. Ghahramanizhad, A. Rezaeifard, *New J. Chem.* **2014**, *38*, 2917–2926.
- [63] M. Haruta, *Chem. Rec.* **2003**, *3*, 75–87.
- [64] E. Rafiee, M. Joshaghani, P. G. S. Abadi, *Res. Chem. Intermed.* **2018**, *44*, 2503–2522.
- [65] K. Sreekumar, T. M. Jyothi, M. B. Talawar, B. P. Kiran, B. S. Rao, S. Sugunan, *J. Mol. Catal. A* **2000**, *152*, 225–236.
- [66] M. Sarno, M. Iuliano, *Appl. Surf. Sci.* **2019**, *474*, 135–146.
- [67] O. Metin, V. Mazumder, S. Ozkar, S. Sun, *J. Am. Chem. Soc.* **2010**, *132*, 1468–1469.
- [68] C. Wang, H. Daimon, Y. Lee, J. Kim, S. Sun, *J. Am. Chem. Soc.* **2007**, *129*, 6974–6975.
- [69] D. Hao, S. Cheng-Min, H. Chao, X. Zhi-Chuan, L. Chen, T. Yuan, S. Xue-Zhao, G. Hong-Jun, *Chin. Phys. B* **2010**, *19*, 066102.
- [70] M. Sarno, M. Iuliano, M. Polichetti, P. Ciambelli, *Process Biochem.* **2017**, *56*, 98–108.
- [71] M. Sarno, E. Ponticorvo, *Int. J. Hydrogen Energy* **2017**, *42*, 23631–23638.
- [72] R. Ramachandran, G. Prakash, S. Selvamurugan, P. Viswanathamurthi, J. G. Malecki, V. Ramkumar, *Dalton Trans.* **2014**, *43*, 7889–7902.
- [73] M. Bala, P. K. Verma, U. Sharma, N. Kumar, B. Singh, *Green Chem.* **2013**, *15*, 1687–1693.
- [74] B. Blank, S. Michlik, R. Kempe, *Chem. Eur. J.* **2009**, *15*, 3790–3799.
- [75] M. Sarno, E. Ponticorvo, C. Cirillo, *J. Phys. Chem. Solids* **2016**, *99*, 138–147.
- [76] M. Sarno, C. Cirillo, E. Ponticorvo, P. Ciambelli, *Chem. Eng. Trans.* **2015**, *43*, 727–732.
- [77] H. E. Ghandoor, H. M. Zidan, M. M. H. Khalil, M. I. M. Ismail, *Int. J. Electrochem. Sci.* **2012**, *7*, 5734–5745.
- [78] X. Sun, C. Zheng, F. Zhang, Y. Yang, G. Wu, A. Yu, N. Guan, *J. Phys. Chem. C* **2009**, *113*, 16002–16008.
- [79] M. Gao, W. Li, J. Dong, Z. Zhang, B. Yang, *World J. Condens. Matter Phys.* **2011**, *1*, 49–54.
- [80] G. Zhou, D. W. Wang, F. Li, L. Zhang, N. Li, Z. S. Wu, L. Wen, G. Q. Lu, H. M. Cheng, *Chem. Mater.* **2010**, *22*, 5306–5313.
- [81] S. Xuan, L. Hao, W. Jiang, X. Gong, Y. Hu, Z. Chen, *Nanotechnology* **2007**, *18*, 035602.
- [82] Z. Xu, C. Shen, Y. Hou, H. Gao, S. Sun, *Chem. Mater.* **2009**, *21*, 1778–1780.
- [83] C. Ban, Z. Wu, D. T. Gillaspie, L. Chen, Y. Yan, J. L. Blackburn, A. C. Dillon, *Adv. Mater.* **2010**, *22*, E145–E149.
- [84] A. Ángeles-Pascuala, J. R. Piñón-Hernández, M. Estevez-González, U. Palc, S. Velumanid, R. Pérez, R. Esparzab, *Mater. Charact.* **2018**, *142*, 237–244.
- [85] S. Moraes Silva, R. Tavalalaie, L. Sandiford, R. D. Tilley, J. J. Gooding, *Chem. Commun.* **2016**, *52*, 7528–7540.
- [86] P. Guardia, S. Nitti, M. E. Materia, G. Pugliese, N. Yaacoub, J. M. Greneche, C. Lefevre, L. Manna, T. Pellegrino, *J. Mater. Chem. B* **2017**, *5*, 4587–4594.
- [87] F. Dumur, A. Guerlin, E. Dumas, D. Bertin, D. Gigmes, C. R. Mayer, *Gold Bull.* **2011**, *44*, 119–137.
- [88] I. Robinson, L. D. Tung, S. Maenosono, C. Walti, N. T. K. Thanh, *Nanoscale* **2010**, *2*, 2624–2630.
- [89] M. Ferrara, H.-C. Neitzert, M. Sarno, G. Gorrasi, D. Sannino, V. Vittoria, P. Ciambelli, *Physica E* **2007**, *37*, 66.
- [90] M. Trezza, S. L. Prischepa, C. Cirillo, R. Fittipaldi, M. Sarno, D. Sannino, P. Ciambelli, M. B. S. Hesselberth, S. K. Lazarouk, A. V. Dolbik, V. E. Borisenko, C. Attanasio, *J. Appl. Phys.* **2008**, *104*, 083917.
- [91] T. Gang, O. Yildirim, S. Kinge, X. Duan, D. N. Reinhoudt, D. H. A. Blank, G. Rijnders, W. G. van der Wiel, J. Huskens, *J. Mater. Chem.* **2011**, *21*, 14800–14806.
- [92] P. Alonso-Cristobal, M. Laurenti, E. Lopez-Cabarcos, J. Rubio-Retama, *Mater. Res. Express* **2015**, *2*, 075002.
- [93] P. Abdulkhin, T. L. Precht, B. R. Knappett, H. E. Skelton, D. A. Jefferson, A. E. H. Wheatley, *Part. Part. Syst. Character.* **2014**, *31*, 571–579.
- [94] E. A. Kwizera, E. Chaffin, Y. Wang, X. Huang, *RSC Adv.* **2017**, *7*, 17137–17153.
- [95] H. Duan, D. Wang, Y. Li, *Chem. Soc. Rev.* **2015**, *44*, 5778–5792.
- [96] A. Fujita, Y. Matsumoto, M. Takeuchi, H. Ryuto, G. H. Takaoka, *Phys. Chem. Chem. Phys.* **2016**, *18*, 5464–5470.
- [97] P. de la Presa, M. Multigner, J. de la Venta, M. A. García, *J. Appl. Phys.* **2006**, *100*, 123915.
- [98] M. Seyhan, W. Kucharczyk, U. E. Yarar, K. Rickard, D. Rende, N. Baysal, S. Bucak, R. Ozisik, *Nanotechnol. Sci. Appl.* **2017**, *10*, 69–77.
- [99] F. Mohammad, T. Arfin, *Adv. Mat. Lett.* **2014**, *5*, 315–324.
- [100] S. Miyano, *Chem. Pharm. Bull.* **1965**, *13*, 1135–1137.
- [101] S. Miyano, A. Uno, N. Abe, *Chem. Pharm. Bull.* **1967**, *15*, 515–517.
- [102] S. Miyano, N. Abe, A. Abe, *Chem. Pharm. Bull.* **1970**, *18*, 511–514.
- [103] S. Miyano, M. Nakao, *Chem. Pharm. Bull.* **1972**, *20*, 1328–1331.
- [104] Y. Horikawa, Y. Uchino, T. Sako, *Chem. Lett.* **2003**, *32*, 232–233.

- [105] A. Bayat, M. Shakourian-Fard, P. Nouri, M. M. Hashemi, *Appl. Organomet. Chem.* **2017**, *31*, e3720.
- [106] A. Mehta, A. Thaker, V. Londhe, S. R. Nanda, *Appl. Catal. A* **2014**, *478*, 241–251.
- [107] M. Klokkenburg, J. Hilhorst, B. H. Erne, *Vib. Spectrosc.* **2007**, *43*, 243–248.
- [108] B. G. Reed-Berendt, K. Polidano, L. C. Morrill, *Org. Biomol. Chem.* **2019**, *17*, 1595–1607.
- [109] N. Chavda, A. Trivedi, J. Thakarda, Y. K. Agrawal, P. Maity, *Catal. Lett.* **2016**, *146*, 1331–1339.
- [110] R. Juárez, S. F. Parker, P. Concepción, A. Corma, H. García, *Chem. Sci.* **2010**, *1*, 731–738.
- [111] B. Chen, L. Wang, S. Gao, *ACS Catal.* **2015**, *5*, 5851–5876.
- [112] J. P. Deng, W. C. Shih, C. Y. Mou, *ChemPhysChem* **2005**, *6*, 2021–2025.
- [113] Q. Peng, Y. Zhang, F. Shi, Y. Deng, *Chem. Commun.* **2011**, *47*, 6476–6478.
- [114] N. Zotova, F. J. Roberts, G. H. Kelsall, A. S. Jessiman, K. Hellgardt, K. K. Hii, *Green Chem.* **2012**, *14*, 226–232.
- [115] H. Yang, R. Mao, C. Luo, C. Lu, G. Cheng, *Tetrahedron* **2014**, *70*, 8829–8835.

---

 Manuscript received: March 22, 2019
 

---